Proceedings of ASME 2022 Internal Combustion Engine Division Forward Technical Conference ICEF 2022 October 16-19, Indianapolis, Indiana, USA

ICEF2022-91113

Combustion characteristics of F24 compared to Jet A in a Common Rail Direct Injection Research Compression Ignition Engine

Valentin Soloiu¹, Richard Smith III¹, Amanda Weaver¹, Drake Grall¹, Cesar Carapia¹, Lily Parker¹, Marcel Ilie¹, Mosfequr Rahman¹

¹Georgia Southern University, Statesboro, GA

ABSTRACT

Research was conducted to determine combustion characteristics such as: ignition delay (ID), combustion delay (CD), combustion phasing (CA 50), combustion duration, derived cetane number (DCN) and ringing intensity (RI) of F24, for its compatibility in Common Rail Direct Injection (CRDI) compression ignition (CI) engine. The first part of this study is investigating the performance of Jet-A, F24, and ultra-low sulfur diesel #2 (ULSD) using a constant volume combustion chamber (CVCC) followed by experiments in a fired CRDI research engine. Investigations of the spray atomization and droplet size distribution of the neat fuels were conducted with a Malvern Mie scattering He-Ne laser. It was found that the average Sauter Mean Diameter (SMD) for Jet-A and F24 are similar, with both fuels SMD droplet range between 25-29 micrometers. Meanwhile, ULSD was found to have a larger SMD particle size in the range of 34-40 micrometers. It was observed during the study, utilizing the CVCC, that the ID and CD for neat ULSD and Jet-A are nearly identical while the combustion of F24 is delayed. F24 was found to have longer durations of both ID and CD by approx. 0.5 ms. This results in a lower DCN for the fuel of 43.5, whereas ULSD and Jet-A have DCNs of 45 and 47 respectively. The peak AHRR for ULSD

and Jet-A are nearly identical, whereas F24 has a peak magnitude of approx. 20% lower than ULSD and Jet-A. It was found that both aviation fuels had significantly fewer ringing events occurring after peak high temperature heat release (HTHR), a trend also observed in the CRDI research engine. Neat F24, Jet-A and ULSD were researched in the experimental engine at the same thermodynamic parameters: 5 bar indicated mean effective pressure (IMEP), 50°C (supercharged and EGR) inlet air temperature, 1500 RPM, start of injection (SOI) 16°BTDC, and 800 bar of fuel rail injection pressure as the baseline parameters in order to observe their ignition behavior, low temperature heat release, combustion phasing, and combustion duration. It was found that the ignition delay of F24 and Jet-A was greater than ULSD, approx. 5% for both aviation fuels. This ignition delay also affected the combustion phasing, or CA 50, of the aviation fuels. The CA 50 of the aviation fuels was delayed by approx. 2% compared to ULSD. Jet-A had a nearly identical combustion duration compared to ULSD, however F24 had an extended combustion duration which was approx. 3% longer than that of ULSD and Jet-A. It was discovered with the accumulations of these delays in ID, CD, CA50, that the RI of the aviation fuels were reduced. F24 was discovered to have more delays, and the RI correlates with these results having a 70% reduction in RI compared to ULSD.

NOMENCLATURE

AHRR – Apparent Heat Release Rate

ATDC – After Top Dead Center

BTDC – Before Top Dead Center

CD – Combustion Duration

CDC – Conventional Diesel Combustion

CI – Compression Ignition

CO - Carbon Monoxide

CO₂ – Carbon Dioxide

CRDI – Common Rail Direct Injection

CVCC – Constant Volume Compression Ignition

DCN – Derived Cetane Number

DI - Direct Injection

DTA –Differential Thermal Analysis

DV (10) – Largest Droplet Size of 10% Fuel Spray

DV (50) - Largest Droplet Size of 50% Fuel Spray

DV (90) - Largest Droplet Size of 90% Fuel Spray

EGR - Exhaust Gas Recirculation

HTHR - High Temperature Heat Release

IC – Internal Combustion

ID - Ignition Delay

IMEP – Indicated Mean Effective Pressure

LTHR - Low Temperature Heat Release

PPRR – Peak Pressure Rise Rate

PRR - Pressure Rise Rate

RI – Ringing Intensity

SFC - Single Fuel Concept

 $\boldsymbol{SMD}-Sauter\ Mean\ Diameter$

SOI – Start of Injection

TGA – Thermogravimetric Analysis

UHC – Unburnt Hydrocarbons

ULSD - Ultra Low Sulfur Diesel

INTRODUCTION

This study has been conducted to observe and compare the behavior of Jet-A commercial aerospace fuel and F24, a non-commercial aerospace fuel, in a Common Rail Direct Injection (CRDI) research engine.

This research was conducted due to the reliance on compression ignition engines for commerce, transportation and power generation. This has led to an effort to study the effects of alternative aerospace fuels for their compatibility within compression ignition engines [1-5].

The idea of using a single fuel for multiple different applications, such as aerospace or on-road transportation, was been devised by NATO after WWII [6, 7, 8]. The initial fuel chosen for the single fuel concept (SFC) was JP-8. In these studies, JP-8 directly replaced ULSD in diesel engines with no other modifications to the platform. It was found that most engines operated successfully [9, 10].

Studies found that JP-8 has the potential to reduce exhaust emissions. This includes the reduction of smoke emissions when directly replacing ULSD in a CI engine. Additionally, it was found that JP-8 produces a favorable shift to the $NO_x - PM$

tradeoff when ample amounts of EGR are added in-cylinder during combustion [11].

The motivation for this study is to evaluate the combustion and emissions of F-24 as a replacement for JP-8 [12]. From the authors' literature review, little to no studies directly comparing F-24, Jet-A and ULSD in an instrumented research diesel engine have been found.

Jet-A is the parent fuel for F-24, with the differences being additives in F-24 for corrosion inhibition, increased lubricity and dissipation of static charge. These additives allow higher altitude flight compared to Jet-A [13, 14]. Furthermore, the fundamental combustion behavior of these fuels are of interest due to their similar DCN, but dissimilar combustion phasing. This will be further studied in the CVCC portion of this study.

Full determinations of the ignition delay (ID), combustion delay (CD), combustion phasing (CA 50), combustion duration and ringing intensity will be analyzed in this study.

Primary investigations include determinations of the research fuel's thermophysical properties and static combustion behavior.

THERMO-PHYSICAL PROPERTIES OF THE SELECTED FUELS

The physiochemical properties analysis of the researched fuels was conducted due to the significant impact these characteristics have on the emissions output and combustion phasing [15-20].

These properties were found experimentally by the use of in-house equipment. These results are contained in Table 1.

Additionally, the equipment used for the physiochemical property analysis and their accuracies are provided in Table 2.

Table 1: Properties of All Researched Fuels

	F24 (19POSF13664)	ULSD	Jet-A (13POSF10325)
Derived Cetane	43.5	47.2	47.0
Number			
Ignition Delay	4.09	3.47	3.36
Combustion	5.79	5.12	5.14
Delay			
Lower Heating	41.85	41.66	41.70
Value			
(MJ/kg)			
Viscosity @	1.37	2.52	1.20
40°C (cP)			
Density [g/mL]	0.835	0.85	0.80
Sauter Mean	18.7	22.8	17.59
Diameter (µm)			
DV (10) μm	9.96	12.5	9.85
DV (50) μm	30.45	40.1	30.11
DV (90) µm	133.33	131.1	133.45

^{*}Derived Cetane Number (DCN) obtained using in house equipment: PAC CID 510 governed by ASTM standard D7668-14a. [21]

Table 2: Physicochemical Analysis Equipment and Accuracies

Instrument	Measured Parameter	Accuracy
Brookfield DV II Pro Rational Viscometer	Viscosity	±1.0%
Parr Constant Volume Calorimeter	Lower Heating Value ±0.3	
Shimadzu DTG-60	Differential Thermal Analysis	±1.0%
	Thermogravimetric Analysis	±1.0%
	Temperature	±1.0%
Malvern Spraytec	Sauter Mean Diameter	±1.0%
PAC CID 510	Derived Cetane Number	±0.3%
	Ignition Delay	±0.1%
	Combustion Delay	±0.1%

Low Temperature Oxidation and Thermal Stability

Shimadzu DTG-60 was utilized for the Α thermogravimetric analysis (TGA) and differential thermal analysis (DTA). Both studies were conducted in an environment of increasing temperature and a constant purge air flow of 15mL/min. The test chamber was heated from approx. 26 °C to 600 °C at a rate of 20°C per minute. Both the TGA and DTA are continuous tests that take approx. 570 measurements of mass, temperature and voltage per minute of run time until the chamber reaches 600°C. For each test, an inert alumina powder was utilized as the baseline, as it loses little to no mass when subjected to high temperatures. This baseline calibrates the apparatus and allows for increased precision during all testing.

Thermogravimetric analysis (TGA) analyzes vaporization of the researched fuels in an environment of increasing temperature. The liquid fuel cannot create a homogeneous mixture with the purge air within the test chamber until it is in a gaseous state [22,23]. The researched fuels are analyzed at the temperature for which 10%, 50% and 90% of the liquid fuel is vaporized (TA 10, TA50 and TA90 respectively) to compare the volatility of the fuels in relation to each other. Of the researched fuels, Jet-A began vaporization at 81.67 °C and was nearly completely vaporized by 163.00°C. F24 needed more heat to vaporize with TA 10 and TA 90 values of 94.9°C and 172.1 °C. Both aviation fuels are much more volatile than ULSD which needs significantly more heat energy from the chamber to completely vaporize. Figure 1 and Table 3 contain the results of the TGA analysis.

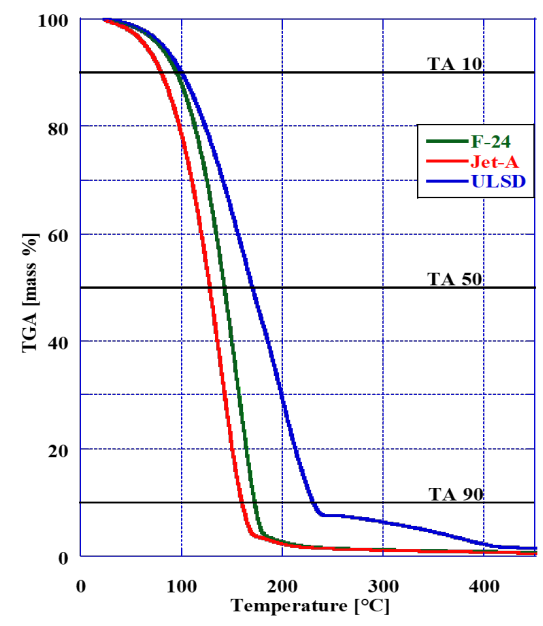


Figure 1: Thermogravimetric Analysis

Table 3: Thermogravimetric Analysis (TA(x))

TA (X) °C	F24	ULSD	Jet-A
TA (10) °C	94.9	110.0	81.67
TA (50) °C	142.1	180.0	129.53
TA (90) °C	172.1	240.0	163.00

The DTA research was conducted to understand the energy release of the researched fuels while in an environment of increasing temperature. Figure 2 and Table 4 contain the results of the DTA determinations of the researched fuels. The negative slopes are periods of endothermic reactions where the fuel is absorbing the heat energy within the test chamber. The positive slopes of the curve are exothermic reactions where the fuels are producing heat energy onto the test chamber. As shown in Figure 2, the aviation fuels absorb and disperse their energy much sooner than ULSD does. Their slopes are much steeper than that of ULSD, signifying that they vaporize much sooner, as indicated in the TGA analysis. The peak of the energy release for F24, Jet-A and ULSD are -19.38 uV/mg, -18.93 uV/mg and -16.87 uV/mg respectively. The aviation fuels of F24 and Jet-A respectively have peak energy released per milligram that are 13.8% and 11.5%, larger than that of ULSD. As the TGA study depicts, nearly all the ULSD and aviation fuels are completely vaporized after approx. 300 °C; however, after 300°C there are more endothermic and exothermic reactions occurring. These reactions are due in some respects because of the additives in the fuels causing these reactions [24-28]. F24 is a high-altitude aviation fuel, compared to ULSD and Jet-A, which are for commercial use. Due to this the additives in the commercial use fuels undergo yet another endothermic and exothermic reaction and their difference come from the notable higher percentage of olefins and cyclohexanes in F24 over Jet-A [42].

Table 4: Peaks of DTA Analysis

	F24	Jet-A	ULSD
Peak DTA	-19.38	18.93	-16.87
(uV/mg)			

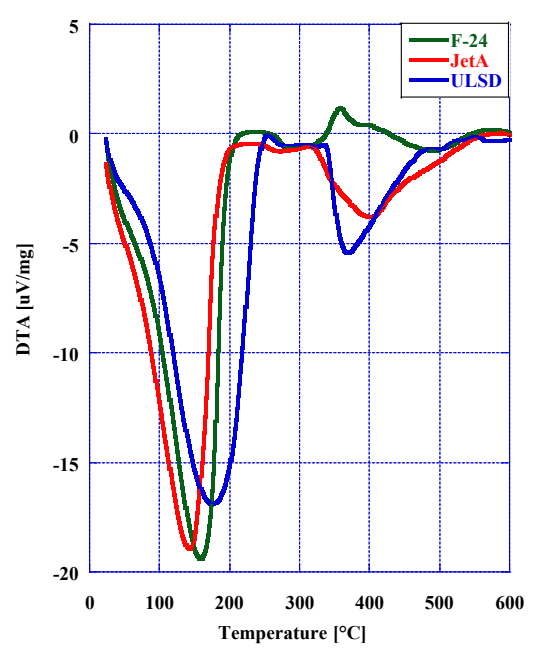


Figure 2: Differential Thermal Analysis

Fuel Spray characteristics investigation with a Mie scattering He-Ne laser

The droplet distributions of an injected fuel spray are paramount to the performance of internal combustion (IC) engines [29,30]. In this study, the spray droplet size and spray distribution analysis of the researched fuels was conducted with a Malvern Spraytec He-Ne laser (632.8 nm wavelength). Fraunhoffer diffraction and Mie scattering theories are utilized to interpret the particle size of the spray droplets through the amount of the beam is diffracted through each individual droplet. The experimental setup for the apparatus is shown in Figure 3. The system consists of a single hole pintle type witness injector, a pneumatic actuation system and Malvern laser. The single hole pintle type injector is chosen for its versatility in both gasoline direct injection and diesel injection systems. The tip of the injector is positioned 100 mm from the He-Ne beam and is injected into the beam perpendicular to the beam with an injection pressure of 180 bar. 28 of the 36 sensors (sensors 8 to 36) are utilized to detect the diffraction caused by the injected fuel as it passes through the beam. The data acquisition of the spray begins 0.1 ms before the measurement trigger and concludes 5ms after the detector is no longer triggered. Data acquisition is measured with a sampling rate of 10kHz with an accuracy of $\pm 0.5 \mu m$. The spray data collection uses the Spraytec software and then is exported to excel for further processing.

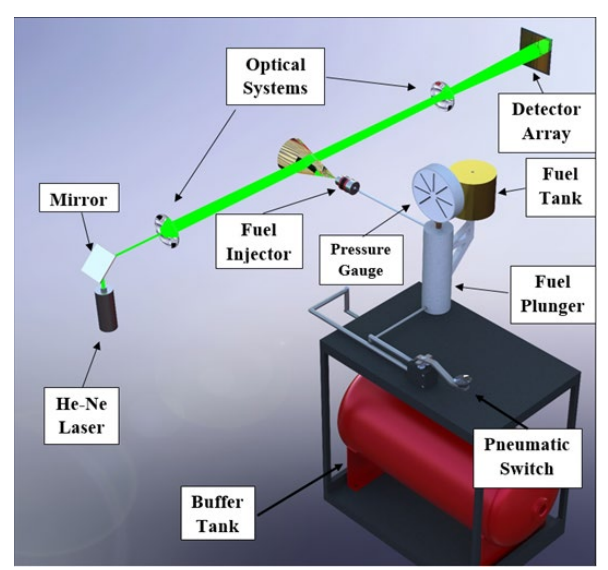


Figure 3: Spraytec Mie Scattering He-Ne laser spray development Analysis Apparatus [31]

The average SMD of the researched fuels as well as the spray volume frequency, measured in % of total injected fuel, is displayed in Figure 4. Jet-A and F24 have nearly identical largest droplet sizes, as denoted as DV in Table 1, (approx. 1% difference) through 10%, 50% and 90% of the spray. The SMD of F24 is 6.1% larger than that of Jet-A, approximately 1.11 μm . ULSD's injection produced larger droplets due to its increased viscosity and density. The DV10 and DV50 for ULSD was 22.6% and 27.3% larger than that of the F24 and Jet-A, the DV 90 was 1.6% lower than that of the aviation fuels. This is potentially due to the rapid vaporization of the aviation fuels. These results reflect the vaporization rates studied in the TGA analysis.

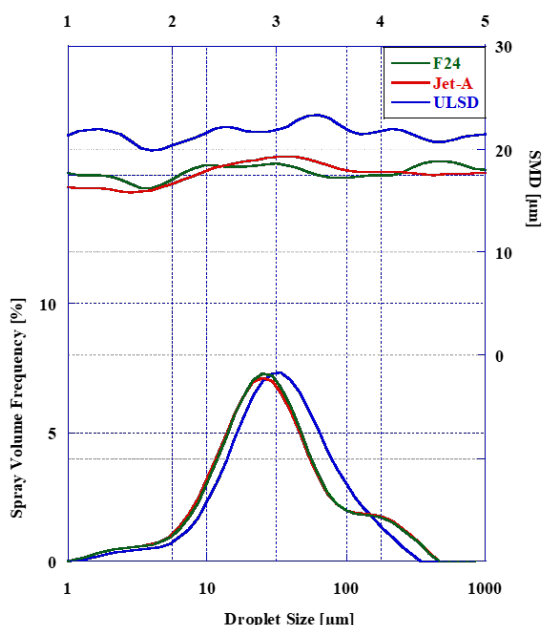


Figure 4: Spray Development of Researched Fuels

CVCC ANALYSIS OF RESEARCHED FUELS

A PAC 510 constant volume combustion chamber using the ASTM D7668-14a. standard, as shown in Table 5 below, for derived cetane number (DCN) determinations was utilized to analyze the fundamental combustion of the researched fuels. A CAD model of the CVCC is displayed on the right in Figure 5. The apparatus is comprised of a high pressure common rail (1), a BOSCH 6 orifice high pressure fuel injector (2), a uniformly heated and pressurized constant volume combustion chamber (3), a Honeywell piezoelectric chamber pressure sensor (4) and an injection pressure sensor (5). The cross-section CAD model is displayed on the left side of Figure 5, this illustrates the spray pattern from the BOSCH injector in the combustion chamber. Data is collected during testing at a rate of 25kHz, or every 0.04 ms for the full 220ms test duration.

Table 5: ATSM D7668-14.a Standard Research Parameters

[21]				
Wall	Fuel	Coolant	Injection	Chamber
Temp.	Injection	Temperature	Pulse	Pressure
	Pressure		Width	
595.5 °C	1000 bar	50 °C	2.5 ms	20 bar

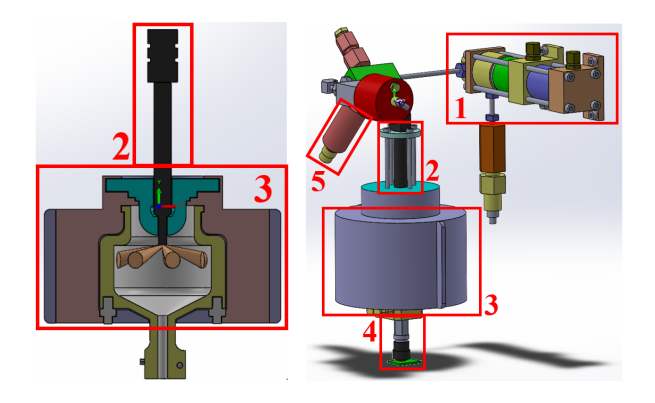


Figure 5: CAD Models of CVCC

For each combustion analysis, 5 conditioning cycles of injection, combustion and exhaust are performed in the CVCC. This is performed to prime the chamber with the test fuel, clear rid any remnants of the previously loaded fuel and stabilize the chamber for the main combustion cycles. 15 main combustion cycles are performed. ID and CD are averaged from these cycles to determine the DCN using Equation 1. The ID, CD and DCN determinations for Jet-A, F24 and ULSD are displayed in Table 6.

$$DCN = 13.028 + \left(-\frac{5.3378}{ID}\right) + \left(\frac{300.18}{CD}\right) + \left(-\frac{12567.90}{CD^2}\right) + \left(\frac{3415.32}{CD^3}\right) \tag{1}$$

Table 6: ID, CD, and DCN of Researched Fuels

	F24	ULSD	Jet-A
DCN	43.35	45	46.99
Ignition	4.09	3.8	3.36
Delay			
Combustion	5.79	5.47	5.14
Delay			

This study includes analysis of the ID, CD, DCN, cool flame formations, negative temperature coefficient region, LTHR region and the HTHR region of the researched fuels. Cool flame formations appear when only a small amount of the reactants in the fuel blend have ignited. It is a period of ignition and quench of the fuel blend [32]. The lightest reactants in the fuel blend ignite but the other reactants have not achieved the amount of energy to ignite, thus they quench the small ignition events.

Following the cool flames region is the negative temperature coefficient region (NTC). This region is caused by the faster dissociation of chain-branching intermediates. Faster dissociation causes a negative correlation between the energy used to decompose these intermediates and aldehydes than the breaking of these bonds creates. This causes the negative slope after peak LTHR.

Once enough of the intermediates and aldehydes have oxidized the HTHR begins and hot flames are rapidly formed. Analysis of these regions are paramount due to their effects on combustion phasing and combustion stabilities [23,36,37]. These regions are defined in Figures 6 and 7.

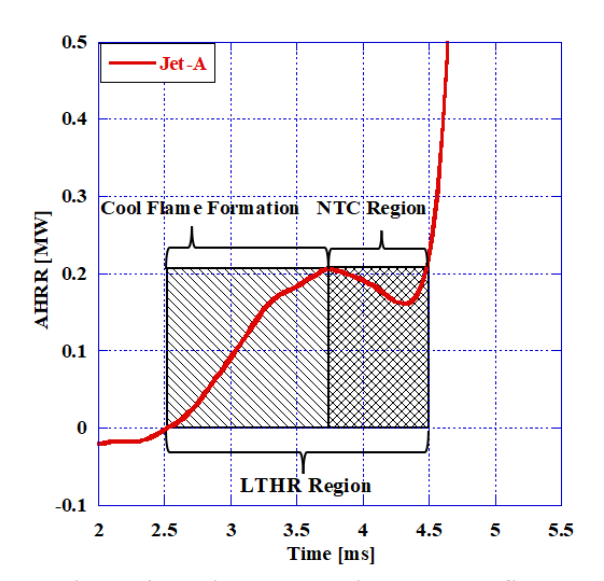


Figure 6: Regions present in LTHR, Defined

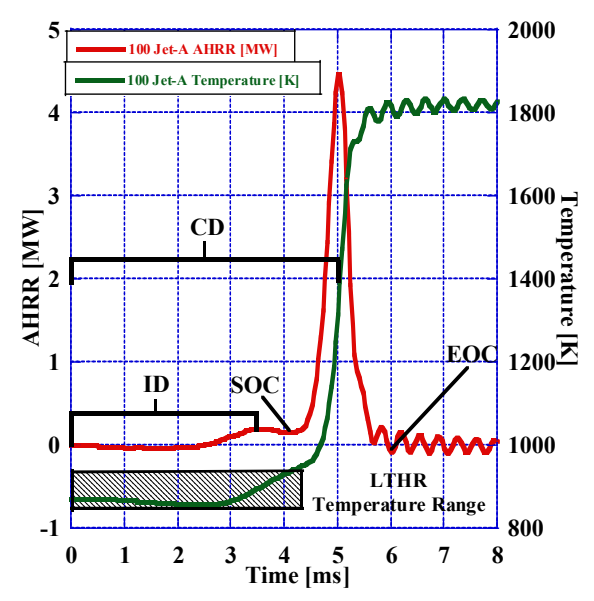


Figure 7: Regions Present in the Full AHRR Analysis,
Defined

In this research, the ID is defined as the period from the start of injection, or 0ms on the following figures, to the peak of the LTHR. The calculations of LTHR begin once the curve of the AHRR rises above 0 after the injection event and continues until the peak AHRR is matched before HTHR, and after the NTC region.

The NTC region starts immediately after peak LTHR and continues until the value for AHRR has reached the peak LTHR directly before HTHR. The temperatures the LTHR region exhibits are approx. between 850K and 950K.

The CD is defined as the period from the start of injection to the peak pressure rise rate (PPRR)/ peak AHRR. Combustion has completed, EOC, when the curve of the AHRR crosses over 0 after peak AHRR for the first time.

Jet-A has the largest value for DCN due to its shortened ID and CD, giving it the best autoignition quality of the researched fuels. The ULSD results are between the aviation fuels results. F24 has the lowest value for autoignition quality with its ID, CD and DCN are approx. 8.5%, 19.0% and 12.0% smaller than that of Jet-A respectively. F24 ID, CD and DCN is lower by approx. 3.7%, 7.35% and 5.7% compared to ULSD respectively. With extended durations of the LTHR region F24 has better combustion stability and a reduced ringing intensity than the other two fuels as shown in the pressure traces and AHRRs of the fuels.

The PAC 510 CVCC measures the dynamic pressure using the pressure sensor in the bottom of the combustion chamber (component 4). The AHRR is analyzed using the first law of thermodynamics. The combustion is considered to occur in a closed system. Additionally, due to the cylinder walls being maintained at a constant temperature of 595.5 °C with no leak through combustion efficiency in the CVCC is considered 100%. The mass of the fuel injected has a percent difference of

less than 2% between each of the researched fuels and each injection produces a homogeneous spray mixture.

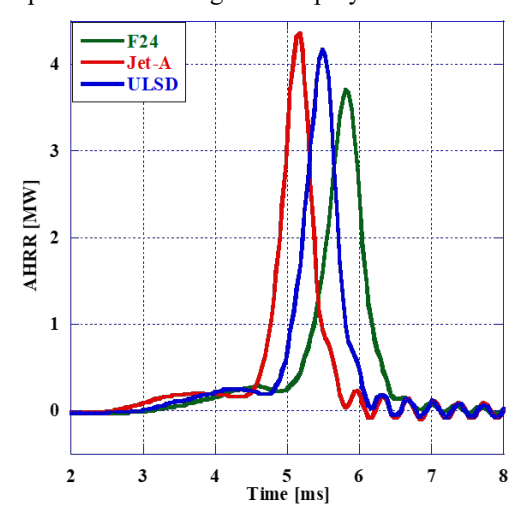


Figure 8: AHRR Analysis of Researched Fuels, CVCC

Jet-A contains the largest autoignition quality of the researched fuels, it also contains the largest AHRR peak that additionally occurs sooner during its combustion cycle, as detailed in Figure 8 and Table 7. The peak AHRR for Jet-A is approx. 15% and 3% larger than F24 and ULSD respectively. Additionally, Jet-A's peak AHRR occurs approx. 12.5% and 6.8% sooner than that of F24 and ULSD respectively.

Table 7: Peak AHRR and Time Occurring

	F24	ULSD	Jet-A
Peak AHRR	3.71	4.18	4.3
[MW]			
Time step [ms]	5.8	5.48	5.12

The LTHR phasing of the three researched fuels are all similar in structure. All the fuels have a distinct peak LTHR, followed by an equally distinct NTC region. Jet-A's cool flame region begins sooner after injection than the other researched fuels and has a shallower slope followed by an extended NTC duration. All the durations are shown in Table 8.

Table 8: CVCC Combustion Phaseing

	Cool Flame Duration/ Beginning of LTHR	NTC Duration	LTHR Duration/End of LTHR
Jet-A	1.24/2.55	0.72	1.96/4.44
F24	1.44/3.21	0.48	1.92/5.00
ULSD	1.68/2.88	0.24	1.92/4.8

Jet-A, with the greatest DCN value, enters the cool flame period earlier than ULSD and F24, entering the phase 2.55 ms after injection, where ULSD and F24 enter the period 2.88 and 3.21 ms after injection respectively. For the entire LTHR period all the fuels had approx. the same LTHR duration of 1.92-

1.96ms; however, the flame propagation of the whole LTHR differed. It was found that longer duration of the cool flame phase resulted in shorter durations of the NTC phase and larger peak LTHR.

The peak LTHR values for Jet-A, F24 and ULSD are 0.20MW, 0.28MW and 0.22MW respectively. Due to the extended cool flame durations more of the peroxides, aldehydes and branch chain intermediates that cause the negative energy correlation are burned in the cool flame formations. This, results in much shorter NTC regions. Figure 9 contains the LTHR regions for each of the researched fuels.

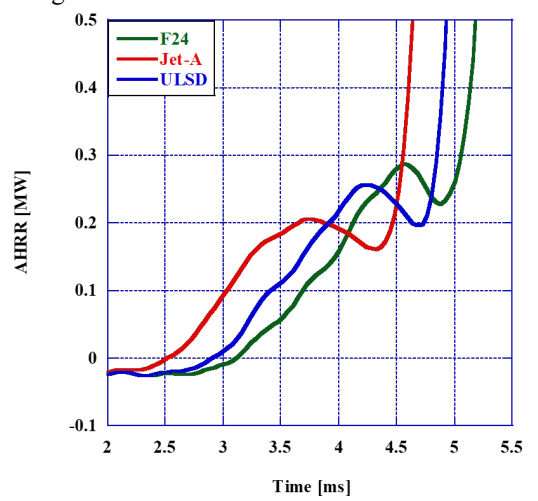


Figure 9: LTHR Duration in CVCC

FIRED CRDI ENGINE METHODS

A 1.1L single cylinder Common Rail Direct Injection (CRDI) research engine was utilized for this investigation. The specifications of the research engine and common rail injector are displayed in Table 9.

An Omron 3600 ppr optical rotary encoder is outfitted on the crankshaft of the engine that is utilized in conjunction with a Compact Rio 9076 Drivven ECU.

Module 9751 controls the engine's injection and timing as well as the common rail pressure and engine speed to achieve the operating parameters for this investigation.

Peak Power	17 kW @ 2200 RPM
Peak Torque	77.5 Nm @1400 RPM
Bore x Stroke	112 mm x 115 mm
Displacement	1.1L
Compression Ratio	16:1
Piston Geometry	Omega bowl in piston
Piezo DI Injection Nozzle	7 orifices x 0.115 mm
Bosch CRDI	800 bar in CDC
Cooling system	Water
Valves per cylinder	2
Supercharger	Pro-charger

A Yokogowa DL850 high speed data acquisition system was used to record and monitor data received from the Omron 3600 ppr rotary encoder for engine position tracking, a Kistler 6053cc Piezoelectric pressure transducer paired with a 5010B dual-mode amplifier was used for in-cylinder pressure monitoring and a Kulite pressure sensor was used for intake pressure monitoring.

All data collected is monitored and averaged over 125 pressure cycles for post processing. An AVL Indicom Flex and Indimodule processed the same data channels from the Yokogowa DL850 for the real-time processing of combustion characteristics and engine performance.

The real time measurements of in-cylinder pressure, pressure rise rate (PRR), coefficient of variation (COV), CA50 and apparent heat release rate (AHRR) are all monitored in real-time using the AVL Indicom. An NI DAQ is utilized to measure the fuel mass flow rate for the common rail direct injection system. This utilized a 213 Maxx Flow meter for raw data collection.

The emissions measured during the fired engine experiments were measured over a span of 2250 engine cycles at a sampling rate of 1Hz. The emissions of nitrogen oxides (NO_x), THC, Formaldehydes, and carbon dioxide (CO₂) were measured with an MKS 2030 21 gas species FTIR emissions analyzer.

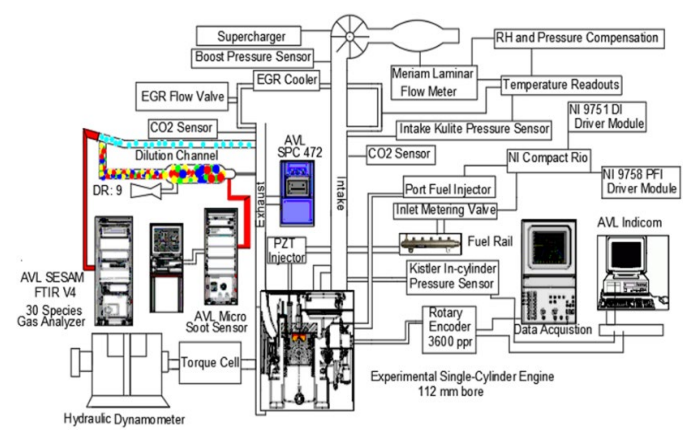
Soot emissions analyzed in this study were collected using AVL Model 483 Micro soot analyzer simultaneously with the MKS 2030 FTIR. Figure 10 below is the experimental setup of the CRDI research engine and Table 10 is the measurement equipment and their accuracies.

Table 10: Fired Engine Equipment and Accuracies

Table 10. Fired Engine Equipment and Accuracies			
Instrument	Measured	Accuracy	
	Parameter		
TQ513 Torque Sensor	Torque	±0.06 %	
Meriam Z50MC2-2	Air Mass Flow Rate	±0.72 %	
Laminar Flow Meter			
213 Maxx Flow Meter	Common Rail Fuel	±0.2 %	
	Flow Rate		
Kulite-175-190 M Intake	Intake Pressure	±0.1 %	
Pressure Transducer			
Kistler 6053cc	In-Cylinder	±0.19 %	
Piezoelectric Pressure	Pressure		
Transducer			
AVL 483 Micro Soot	Soot Concentration	±3.8 %	
Sensor			
MKS FTIR 2030	NO _X , UHC, CO,	±2.0 % of	
	CO_2	PPM Auto	
		range	

Figure 10: Experimental CRDI Engine

The fired engine analysis includes examinations of the ignition delay, combustion duration, combustion phasing (CA50), and ringing intensity (RI) for all the researched fuels under different operating parameters (20% EGR added and 0.28 bar of boost).



The baseline parameters for all testing includes an engine RPM of 1500, SOI of 16° before top dead center (BTDC), an IMEP of 5 bar, 50°C inlet air temperature, and a fuel rail pressure of 800 bar. The pulse width of the injection is dependent on the researched fuel and operating parameters. The pulse width is controlled with the Drivven ECU to keep the IMEP constant for all experiments. For baseline, each fuel operated at these conditions with no added boost or EGR, and this was denoted in this research as Conventional Diesel Combustion (CDC). The fuels will also have tests with either 20% EGR added, or 0.28 bar of boost added, these are denoted with EGR or boost in all the graphs and Tables used.

Combustion Pressure Analysis

In-cylinder pressure is measured during all engine experiments. This data is broken into three different sets of tests denoted CDC, EGR and boost. The in-cylinder pressures over CAD and peak pressures are displayed in Fig. 11,12,13 below. A motoring curve is included in the Figures for reference and the beginning of the cycle is set at the start of the intake stroke.

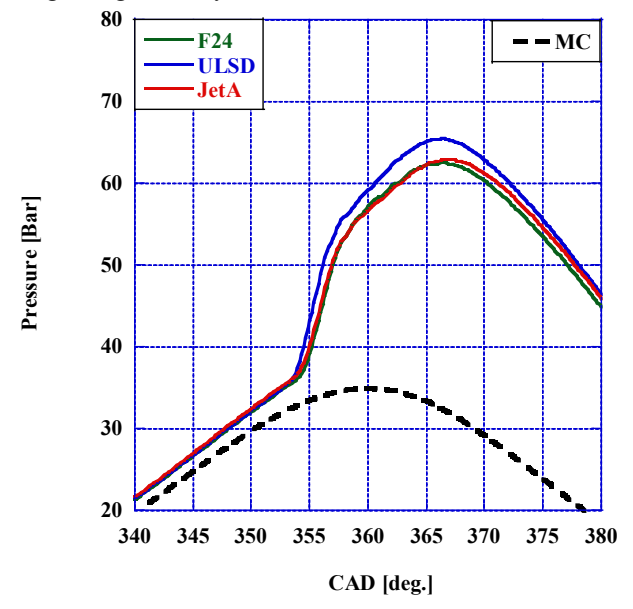


Figure 11: CDC Combustion Pressure

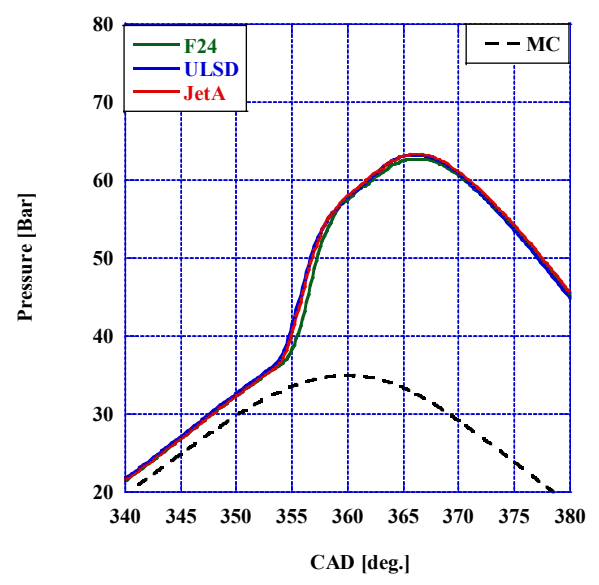


Figure 12: Combustion Pressure with 20%EGR

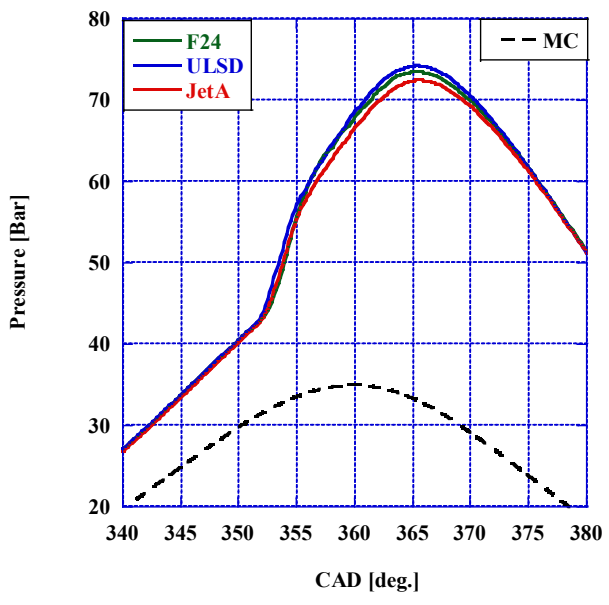


Figure 13: Combustion Pressure with Boost

It was discovered that ULSD's pressure trace is the most affected by EGR and boost compared to the aviation fuels. The aviation fuels maintained approximately the same pressure trace throughout experimentation.

ULSD has a lower peak when EGR is added and produced a larger and sharper peak when boost is applied.

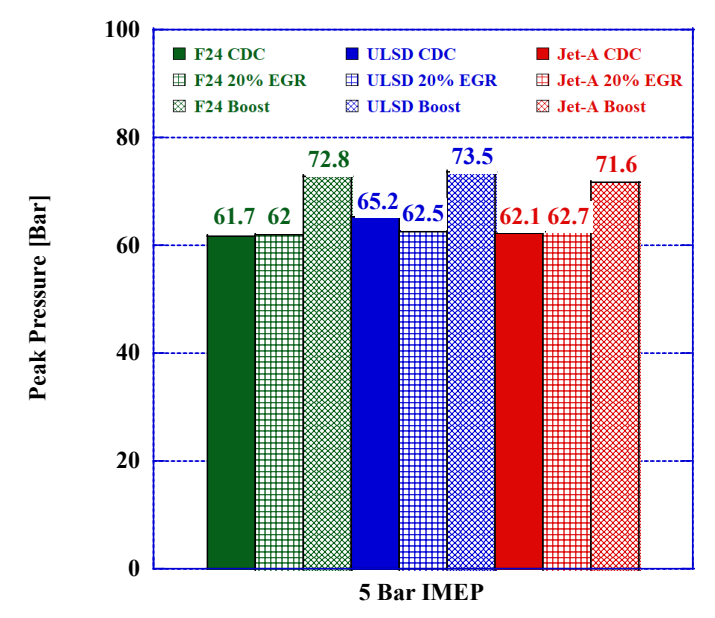


Figure 14: Peak Combustion Pressures

The peak pressures of F24 in all combustion modes were lower than that of ULSD by 3.5 bar, 0.5 bar and 0.7 bar for CDC, EGR, and boost respectively. Jet-A's peak pressures were lower than that of ULSD in CDC mode and boosted mode by 3.1 and 1.9 bar respectively; however, during combustion with EGR added, Jet-A had a larger peak pressure than ULSD by 0.2 bar.

Table 11 depicts the CAD increment of each peak pressure that takes place during the combustion cycle.

Table 11: Peak Pressure Location in the Cycle

Fuel and Combustion Method	Peak Pressure Location
	[CAD]
ULSD CDC	366.36
ULSD EGR	366.18
ULSD Boost	364.92
F24 CDC	366.54
F24 EGR	366.18
F24 Boost	365.46
Jet-A CDC	370.0
Jet-A EGR	366.0
Jet-A Boost	366.19

F24's peak pressure occurs later in the combustion cycle than that of ULSD for CDC and boosted modes and is identical to that of USLD in EGR mode; however, these delays are less than 1° CAD in comparison. F24's peak pressure occurs before that of Jet-A in CDC and Boost modes but trails in EGR mode. This is all by less than 1° CAD

Pressure Rise Rate Analysis

During the CDC combustion mode, as shown in Figure 15, ULSD had the greatest peak PRR of 7.19 bar/CAD. The peak of ULSD occurred significantly earlier than that of the aviation

fuels. Additionally, the duration of the PRR over the combustion event is longer than that of the aviation fuels. Jet-A and F24 are nearly identical for the CAD the PRR begins its sharp increase.

Jet-A resulted in a larger value for PRR of 6.33 bar/CAD than F24's value of 6.11 bar/CAD; however, F24 is observed to have an extended plateau for PRR at approx. 5.8 bar/CAD that is longer in duration than that of Jet-A's curve.

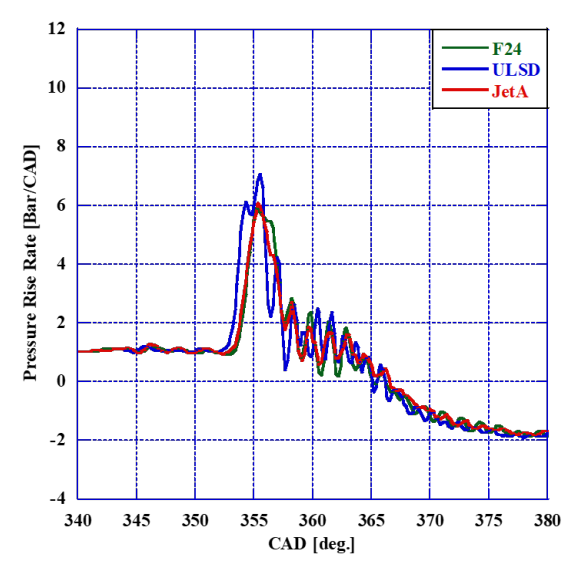


Figure 15: Pressure Rise Rate, CDC

The EGR additions delay the ignition of F24 so that the fuel's PRR increases substantially due to accumulation of fuel in the combustion chamber, as seen in Figure 16. The closer the beginning of the fuel's ignition is to TDC the larger the pressure rise rate and shorter the duration of this pressure rise.

This is a significantly later pressure rise compared to that of ULSD and Jet-A. It is apparent in EGR combustion mode that Jet-A and ULSD have periods of sustained PRR whereas F24 has one event occurring closer to TDC with a shorter duration.

In the boosted modes both aviation fuels ignite closer to TDC with ULSD being the earliest, followed by Jet-A and F24 as the latest to have a sharp PPR increase. Jet-A is observed to have the smallest peak in boosted mode but has an extended durations of PRR as seen in Figure 17. F24 endures the same PRR trace as EGR mode with late ignition and sharp, high peak and short PRR duration.

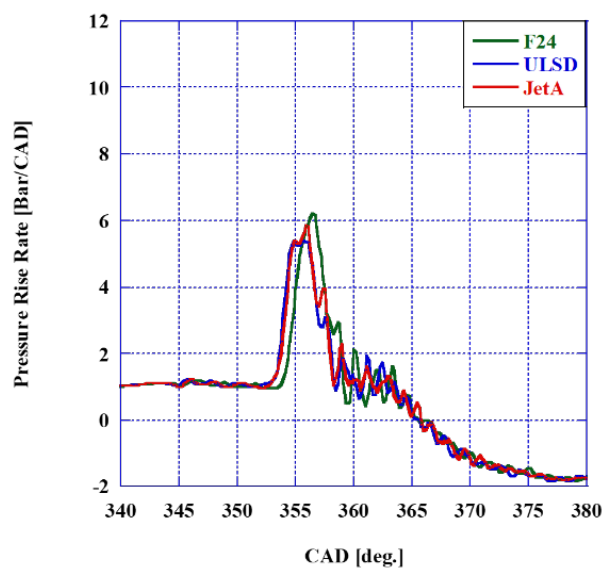


Figure 16: Pressure Rise Rate, EGR

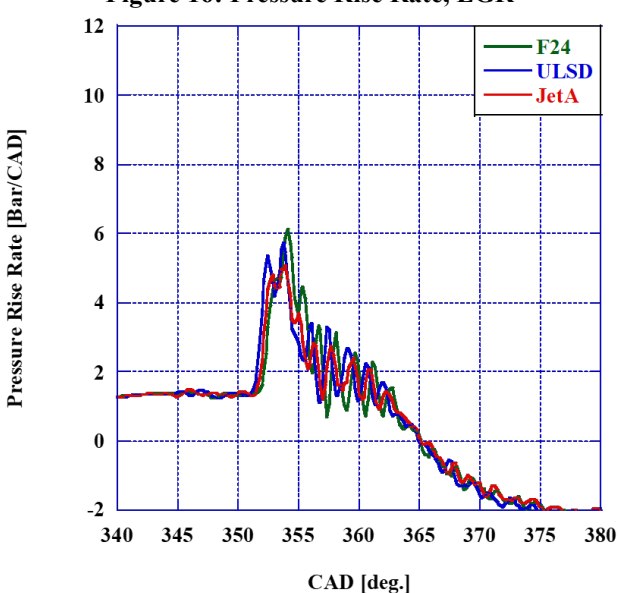


Figure 17: Pressure Rise Rate, Boost

It was found that the PPR peaks of the aviation fuels had an inverse correlation to each other when compared to the combustion modes in which they were researched, as displayed in Figure 18. Where F24's PRR peak became larger through EGR mode and boosted modes, compared to CDC mode; Jet-A PRR peaks became lower than CDC through the additions of EGR and boost. F24 peak PRR was larger than that of ULSD and Jet-A for EGR and boosted modes and the lowest PRR through the CDC mode.

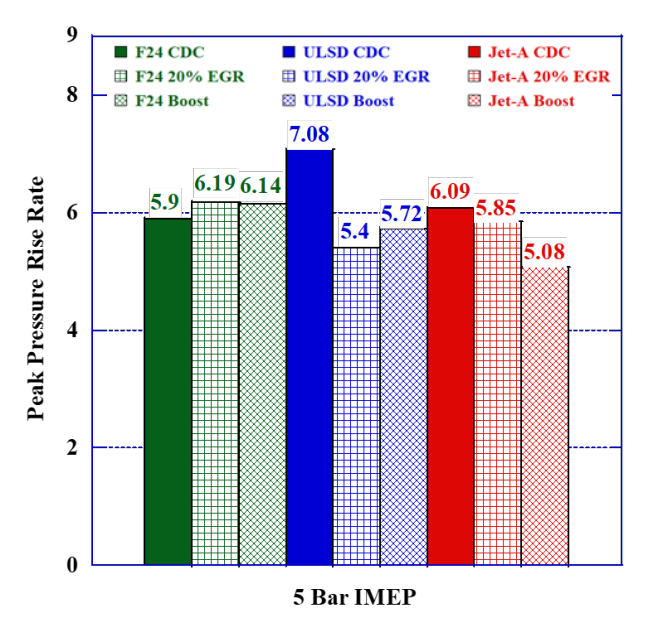


Figure 18: Peak Pressure Rise Rate

Ringing Intensity Analysis

The Ringing Intensity (RI) analysis for all the combustion experiments utilized Equation 2 below. This equation requires the use of Peak PRR, maximum temperature, and peak pressure of the averaged cycles [22].

$$RI = \frac{(\beta(\frac{dP}{dt})_{max})^2}{(2\gamma P_{max})} \sqrt{\gamma R T_{max}}$$
 (2)

The results of the RI analysis are shown in Figure 19. Jet-A yielded reduced ringing compared to ULSD in all combustion modes, wherein the boosted combustion mode it yielded a 50% reduction in RI and in BSFC, as will be discussed later in this paper. F24 had a significant reduction in RI compared to ULSD in CDC and EGR modes, reductions of approx. 70% and 28% respectively.

F24 had an additional reduction in RI compared to that of Jet-A with reductions in CDC and EGR modes of 18.6% and 9.2% respectively. However, in boosted applications F24 had an extreme increase in RI as opposed to ULSD and Jet-A which had increases of 44.4% and 86.4% respectively. Of all the fuels ULSD had the largest peak RI of 1.74 in the CDC combustion mode. The largest peaks in the PRR analysis correlate to the largest RI peaks.

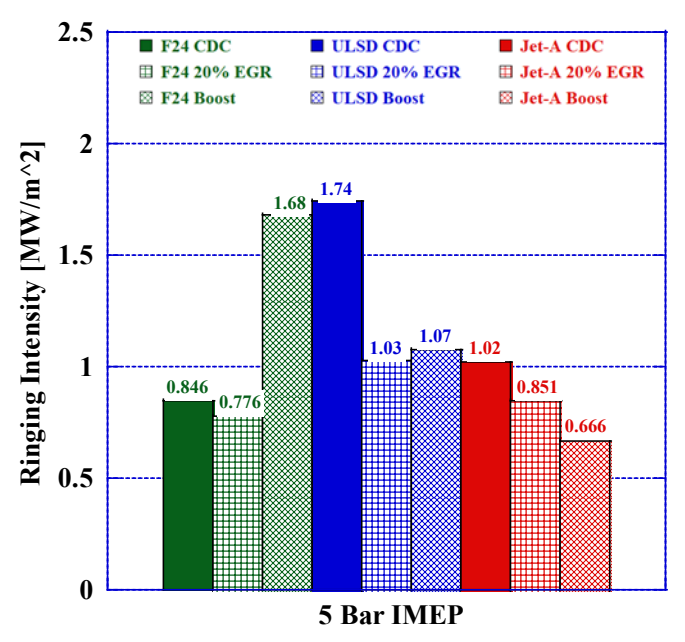


Figure 19: Peak Ringing Intensity

Apparent Heat Release Analysis

The apparent heat release analysis (AHRR) is calculated using the first law of thermodynamics. The combustion in this study is treated as it is occurring in a closed system. The equation utilized for the AHRR analysis/simulation is presented below:

$$\frac{dQ}{d\theta} = \frac{1}{[\gamma - 1]} V \frac{dP}{d\theta} + \frac{\gamma}{[\gamma - 1]} P \frac{d\nu}{d\theta}$$
 (3)

In CDC combustion mode ULSD has the largest peak AHRR with a value of 105.0 J/CAD. Additionally, ULSD begins its HTHR phase earlier than that of the aviation fuels. Both Jet-A and F24 have similar Ignition delays and similar flame propagation through the CDC combustion analysis, as seen in Figure 20. Neat F24 and Jet-A had an identical ID (CA10) of 4.3°BTDC and a similar CA 50 of 9.42 and 9.06 after top dead center (ATDC) respectively. F24 had a slightly longer duration through its combustion phasing, reaching 90% of the fuel burned at 42.36°ATDC. Jet-A reached 90% of the fuel burned at 41.28 °ATDC. ULSD began earlier in the combustion cycle and concluded earlier with a CA 10, 50 and 90 of 4.84°BTDC, 9.24° ATDC and 41.46°ATDC respectively.

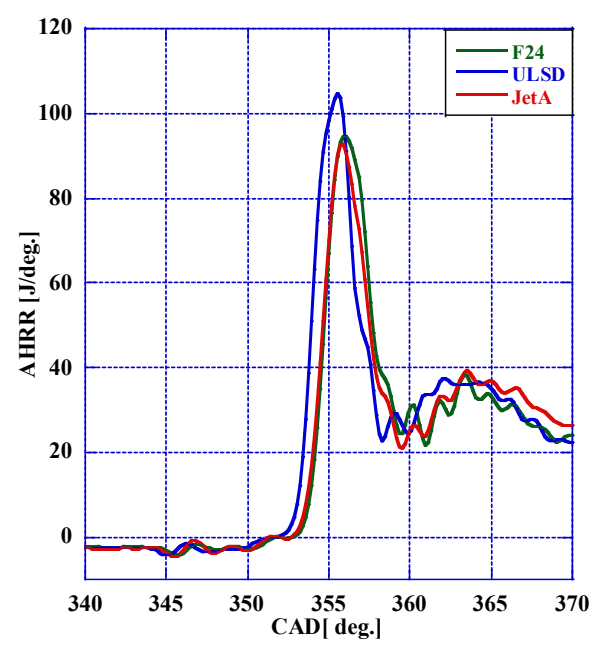


Figure 20: AHRR, CDC

Jet-A and ULSD, unlike the CDC combustion AHRR, had very similar EGR combustion phasing, as seen in Figure 21. Jet-A achieved a slightly higher peak than that of ULSD with a peak value of 91.2 J/CAD compared to ULSD which achieved a peak value of 87.0 J/CAD. The combustion phasing was similar with identical CA10 and CA50 values of 4.48 °BTDC and 8.70 ATDC. Jet-A had a longer combustion duration to reach 90% fuel burn (CA 90) which was achieved 42.54 °ATDC as opposed to ULSD which achieved the CA 90 mark at CAD of 42.18°ATDC. F24 ignited significantly later than that of Jet-A and ULSD with a CA 10 of 3.94 BTDC.

This ignition was closer to TDC causing the slope of the AHRR to incline into HTHR in a more rapid fashion. This is due to the higher temperature and pressures present as the piston is reaching TDC. The CA50 of F24 was achieved at 8.88 °ATDC. However, even though F24 ignited and entered its HTHR phasing closer to TDC, the combustion duration from CA10 to CA 90 was identical to that of ULSD, with a value of 46.62°CAD. Jet-A achieved a combustion duration of 46.98°CAD.

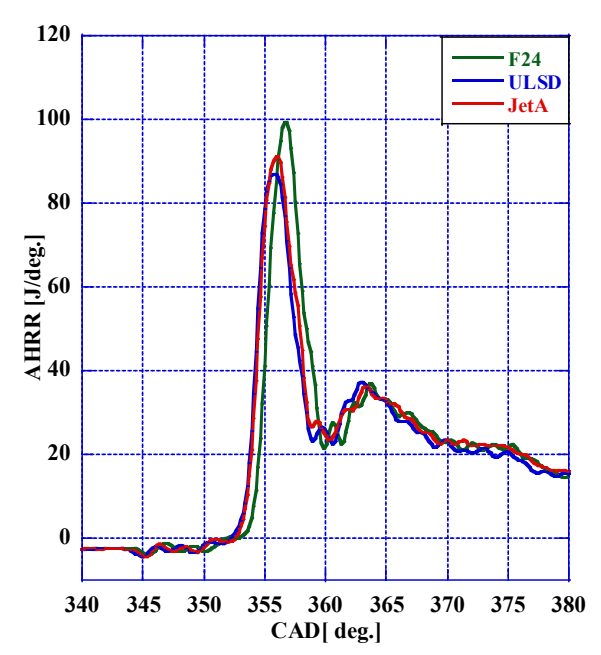


Figure 21: AHRR, EGR

When 0.3 bar of boost is added all the fuels have their peak AHRR occur earlier than the other combustion methods as seen in Figure 22. Additionally, the combustion durations were reduced with F24, Jet-A and ULSD achieving combustion durations of 44.0°, 43.92° and 44.28°. F24 was the least susceptible to boost pressures increasing with its ignition delay being only 0.45° (4.75ATDC) difference compared to the ID during CDC mode (4.3° ATDC). Jet-A and ULSD had their ID begin much earlier in the stroke compared to CDC by approx. 2 CAD for both fuels.

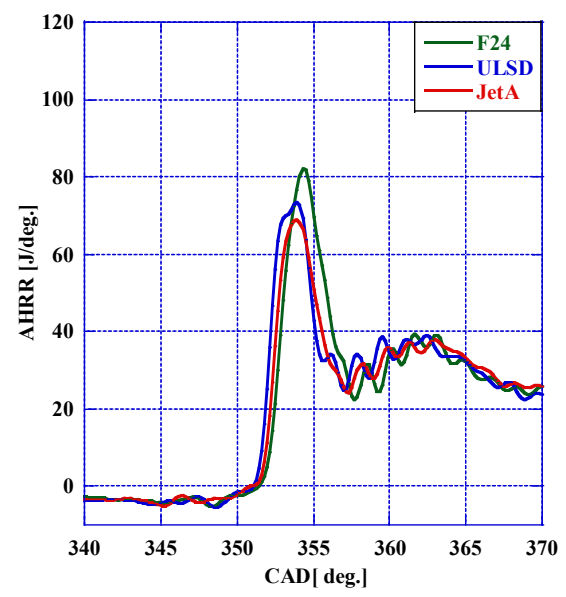


Figure 22: AHRR, Boosted

With the SOI occurring at 16°BTDC (344° CAD), there is a small drop in AHRR at approx. 345° - 350° CAD. This small drop is due to the fuel entering the chamber and absorbing the surrounding heat energy that is already present in the combustion chamber. This event is then followed by the formation of cool flames and the low temperature heat release region [32]. The period of cool flames occurred at approx. 345°CAD until the HTHR event. The positive and negative slopes in the AHRR curve before the HTHR are the periods of ignition and quench produced by the formation of cool flames in the LTHR region.

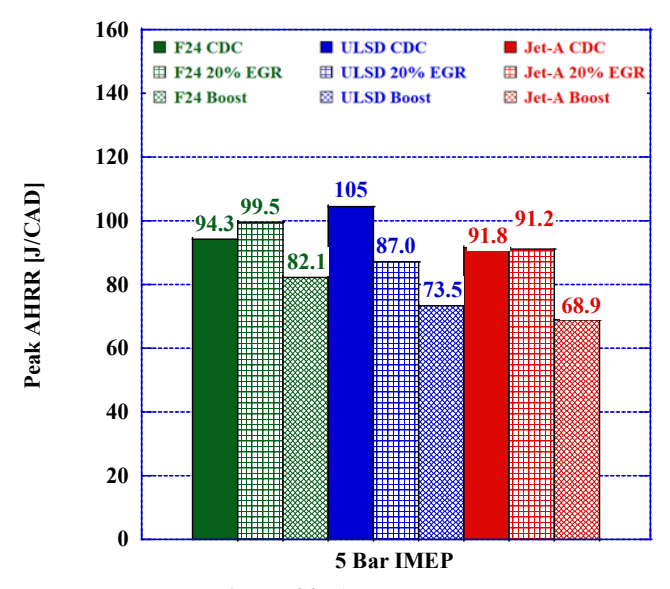


Figure 23: AHRR Peaks

The reduced AHRR peaks in the boosted applications are due to a reduced injection pulse width, thus lesser amounts of fuel delivered into the combustion chamber, for the research engine to maintain the 5 bar IMEP load, as seen in Figure 23. This is apparent across all the boosted tests. No other parameters are changed except the injection pulse width which is controlled automatically with the Drivven ECU.

The CA10, CA50, CA90 and combustion duration for each fuel and each experiment is displayed in Table 12.

Table 12: CA10, CA50, CA90 and Combustion Duration of all Experiments

Experiment	CA10 After SOI/ TDC		CA50 After SOI/ TDC		CA90 After SOI/ TDC		Comb. Duration (CA10 to CA90)
F24 CDC	11.7	4.30 BTDC	25.1	9.06 ATDC	58.4	42.36 ATDC	46.62
F24 EGR	12.0	3.94 BTDC	24.9	8.88 ATDC	58.7	42.72 ATDC	46.62
F24 Boost	11.2	4.75 BTDC	24.1	8.16 ATDC	55.3	39.3 ATDC	44.00
ULSD CDC	11.1	4.84 BTDC	25.2	9.24 ATDC	57.5	41.46 ATDC	46.26
ULSD EGR	11.5	4.48 BTDC	24.7	8.70 ATDC	58.2	42.18 ATDC	46.62
ULSD Boost	9.5	6.46 BTDC	23.2	7.26 ATDC	53.5	37.5 ATDC	43.92
Jet-A CDC	11.7	4.30 BTDC	25.4	9.42 ATDC	57.3	41.28 ATDC	45.54
Jet-A EGR	11.5	4.48 BTDC	24.7	8.70 ATDC	58.5	42.54 ATDC	46.98
Jet-A Boost	9.9	6.10 BTDC	24.1	8.16 ATDC	54.2	38.22 ATDC	44.28

In-Cylinder Combustion Temperature

The in-cylinder combustion temperature for the researched fuels and their combustion modes are displayed in Figures 24, 25, and 26. Additionally, the peak temperatures are provided in Table 13. In CDC and boosted combustion modes ULSD combusts at higher temperatures compared to F24 and Jet-A. With EGR added, Jet-A has the highest temperature at 1166.1 °C, with F24 next hottest with a temperature of 1147.8 °C and ULSD burning the coolest at EGR with a peak temperature of 1135.1 °C.

Comparing CDC and EGR combustion temperatures, it is apparent that ULSD is more susceptible to the different combustion modes compared to the aerospace fuels. For all the research fuels they had their largest peak temperature while in CDC mode and their lowest peak temperature in EGR combustion mode. While in CDC and EGR modes, ULSD's peak temperature is 1298.6 °C and 1135.1 °C, respectively. This is a difference of approx.163 °C respectively. Where Jet-A and F24 had differences of approx. 117°C and 106°C, respectively. This is an indication that the aerospace fuels' combustion is less susceptible to change depending on if extra oxygen is added in cylinder in boost mode, or if less oxygen is present when EGR is added.

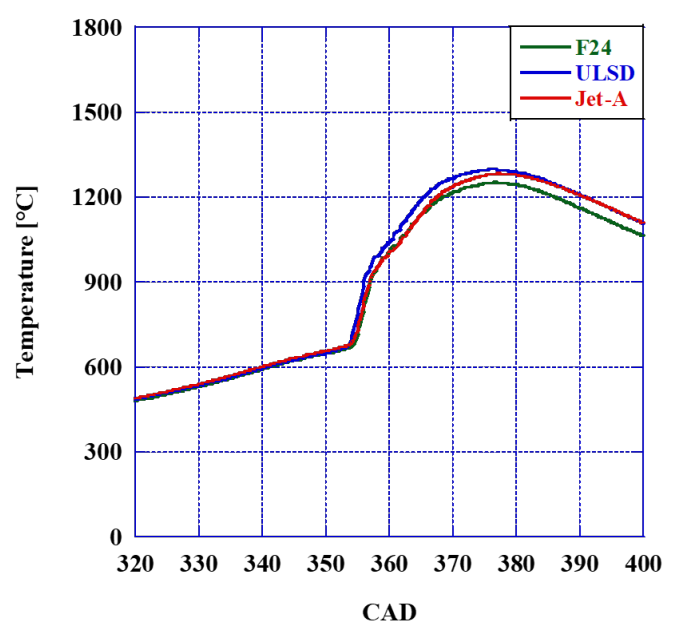


Figure 24: In-Cylinder Temperature, CDC

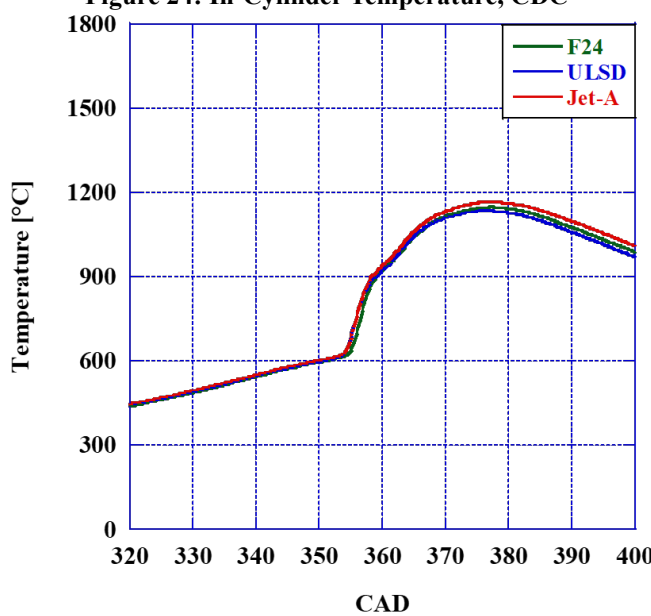


Figure 25: In-Cylinder Temperature, 20% EGR

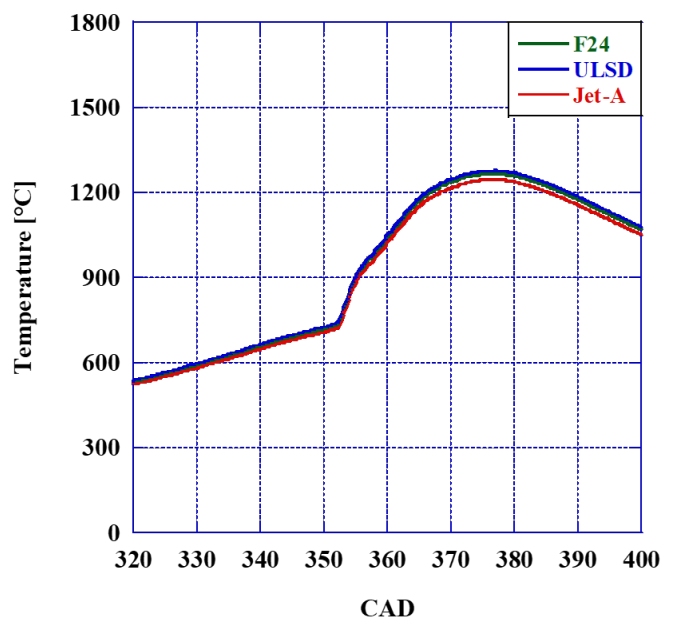


Figure 26: In-Cylinder Temperature, Boosted

Table 13: Peak In-Cylinder Temperature

Fuel and Combustion Method	Peak In-Cylinder Temperature [°C]
F24 CDC	1253.0
F24 EGR	1147.8
F24 Boost	1267.4
ULSD CDC	1298.6
ULSD EGR	1135.1
ULSD Boost	1277.8
Jet-A CDC	1282.9
Jet-A EGR	1166.1
Jet-A Boost	1246.6

Emissions Analysis

The instrumented CRDI research engine did not use any after-treatment systems for any of the emissions analysis. An after-treatment system was not implemented into the engine to closely observe the in-cylinder emissions produced by the various combustion experiments.

An MKS 2030 was utilized to measure the gaseous emissions of NO_x, CO and CO₂. An AVL Microsoot, Model 483, was utilized to measure the soot emissions, in real time, during all the combustion experiments.

NO_X Emissions

The NO_x analysis showed that by adding the EGR the flame propagation slowed down and AHRR diminished for all fuels. The PRR has been lowered and the in-cylinder peak temperature has been drastically reduced [33, 34]. For those

reasons the NOx emissions have been reduced with EGR for all fuels.

Meanwhile, when boost was added, the air excess was increased with more nitrogen available to react as seen in Figure 27. F24 had increases of approx. 10% more NO_x emissions compared to ULSD in CDC and EGR combustion modes. Jet-A had additional increases of 21.9% and 31.4% compared to that of ULSD in CDC and EGR modes. Both aviation fuels had reductions when boost was added with F24 and Jet-A having reductions of 13.8% and 2.1% compared to that of ULSD.

Usually, NO_x emissions are dependent on in-cylinder temperature, where an increase in in-cylinder temperatures cause an exponential increase in NO_x emissions [33, 34].

In this study the opposite occurred during the CDC and EGR combustion modes. ULSD had the highest in-cylinder temperatures through most of the combustion event, however it achieved lower emissions in the CDC and EGR combustion modes compared to the aerospace fuels. In the boosted modes, the aerospace fuels produce a significantly lower amount of NO_x emission than that of ULSD

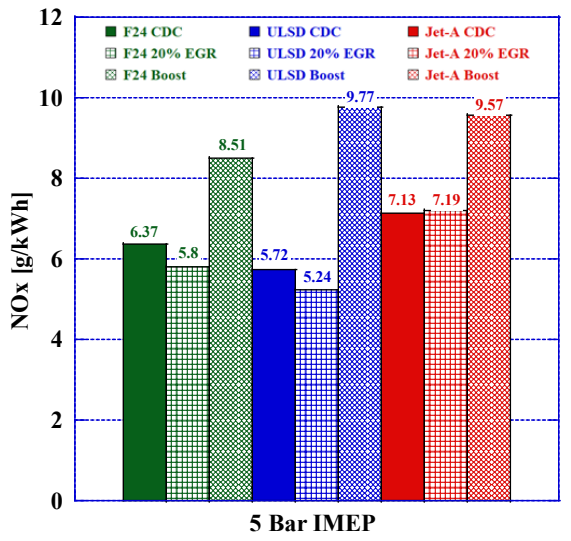


Figure 27: NO_x Emissions.

CO Emissions

The CO emissions followed the same trend as the NO_x . These emissions are produced when the combustion reaction isn't fully completed [35]. The aerospace fuels react and have more complete combustion when there is boost added incylinder. This addition of more oxygen aids in completing the full combustion reaction for the aerospace fuels.

Compared to ULSD, the aviation fuels F24 and Jet-A had increases of carbon monoxide (CO) emissions by 17.1% and 3.6%, respectively, in the CDC combustion mode. F24 and Jet-A had also increased when boost was added, these increases were in amounts of 34.9% and 38%, respectively, as seen in Figure 28. With EGR added F24 experienced a 6.1% reduction in CO when compared to ULSD; however, Jet-A experienced a 15.7% increase.

Jet-A emitted approx. 21.8% more CO than that of F24 with EGR added and was nearly identical in CO outputs compared to F24 when boost is applied.

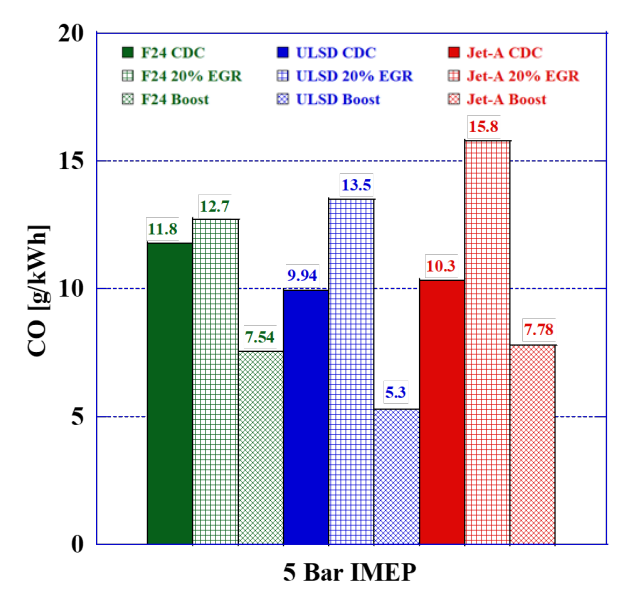


Figure 28: CO Emissions

CO₂ Emission

Carbon dioxide emissions are of large importance in this study due to contribution to climate change as a greenhouse gas. Thus, investigating the use of aviation fuels in a CI engine for their CO_2 outputs are paramount for the viability of F24 and Jet-A in a CRDI engine.

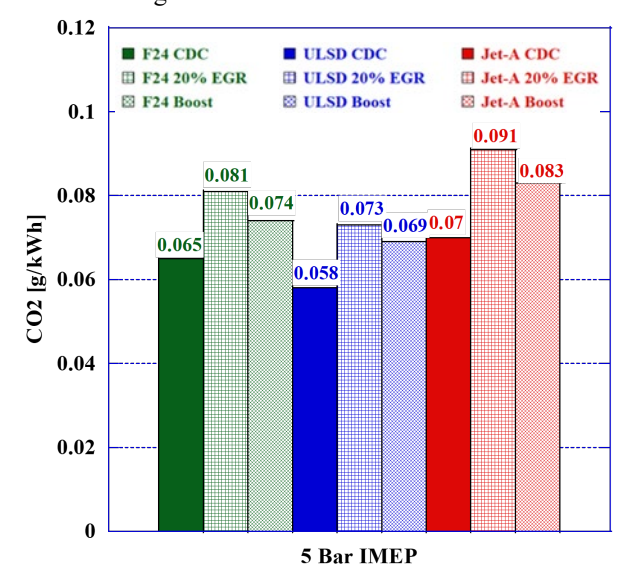


Figure 29: CO2 Emissions

 CO_2 outputs produced by the aviation fuels were larger than that of ULSD in all combustion modes and both fuels as seen in Figure 29. F24 had increases in CO_2 outputs in amounts of 11.4%, 10.4% and 7.0% in CDC, EGR and boosted combustion modes larger than ULSD respectively.

Jet-A performed worse than that of F24 with increases, compared to ULSD, of 18.8%, 22.0% and 18.4% in CDC, EGR and boosted modes respectively.

All the fuels followed the same trend with their CO_2 emissions. The trend being that in EGR mode the CO_2 emissions were the highest, CDC mode the emissions lowest and in boosted mode the emissions were in between that of EGR and CDC mode. This is due to the EGR further reducing the flame propagation for the aviation fuels.

SOOT Emission

F24 and Jet-A performed significantly better with regards to ULSD in soot emissions as seen in Figure 30. Out of all experimentation, F24 had a 9.2% increase in soot emissions compared to that of ULSD in CDC. In all other experiments the aviation fuels performed better than that of ULSD. In EGR mode F24 had reductions of 19.6% and 5.5% for the EGR and boosted combustion modes respectively. Jet-A had soot reductions across all testing compared to ULSD with reductions of 8.2%,34.1% and 6.3% across the CDC, EGR and boosted combustion modes. Additionally, Jet-A performed better than that of F24 with reductions of 0.2, 0.24 and 0.005 g/kWh across the CDC, EGR and boosted modes.

The in-cylinder temperature for Jet-A was lower than that of all the researched fuels in this study. Likewise, it has the lowest soot emissions of all the researched fuels in this study because the in-cylinder temperature is related to this reduction in soot outputs. ULSD has the highest temperatures and has the largest amount of soot emissions over EGR and boosted combustion modes but is lower than F24 in CDC mode.

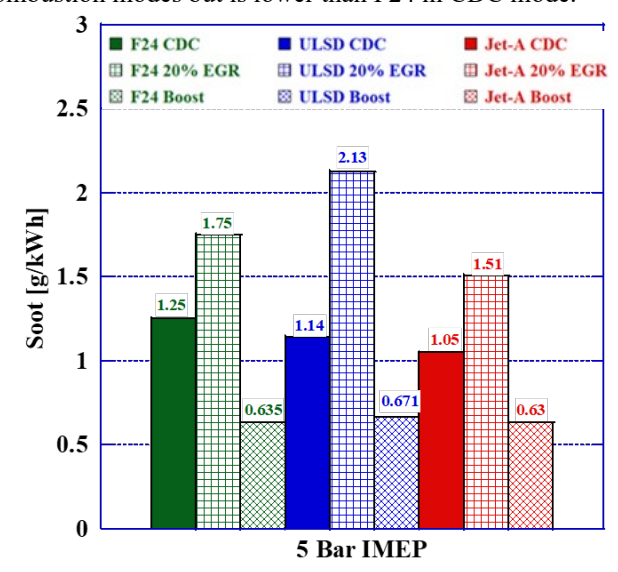


Figure 30: Soot Emissions

The increased amount of soot production from F24 may be caused by the increased amount of fuel that needed to be injected into the cylinder to maintain the 5 bar IMEP load. The

fuel flow rate of F24 in the CDC combustion mode is 1.11 Kg/hr, which was the largest fuel flow rate of all experiments. A further analysis of the direct injection fuel flow for each experiment will be discussed later in this manuscript.

Break Specific Fuel Consumption

The BSFC of the researched fuels is closely related to the LHV because it is an important metric for the energy density of the fuel [38-41]. Due to both aviation fuels having higher LVH values than that of ULSD with F24 and Jet-A having values of 41.85 and 41.7, respectively, compared to ULSD's LHV of 41.66. The fuel flow rate of each of the fuels are also identified in Table 14. As seen in Figure 31 the BSFC closely relates to the fuel flow rate, where Jet-A has the best performance with needing the least amount of injected fuel to maintain the 5 bar IMEP load applied to the engine.

Jet-A matched BSFC with ULSD in CDC mode and had better values for EGR and boosted combustion with reductions of 4.3% and 1.75%. F24 required more injected fuel load applied to the CRDI research engine, resulting in increases of 5.8% and 3.4% of fuel consumption compared to ULSD in CDC and boosted combustion modes. F24 matched ULSD's fuel consumption when additions of 20% EGR is introduced to the CRDI engine.

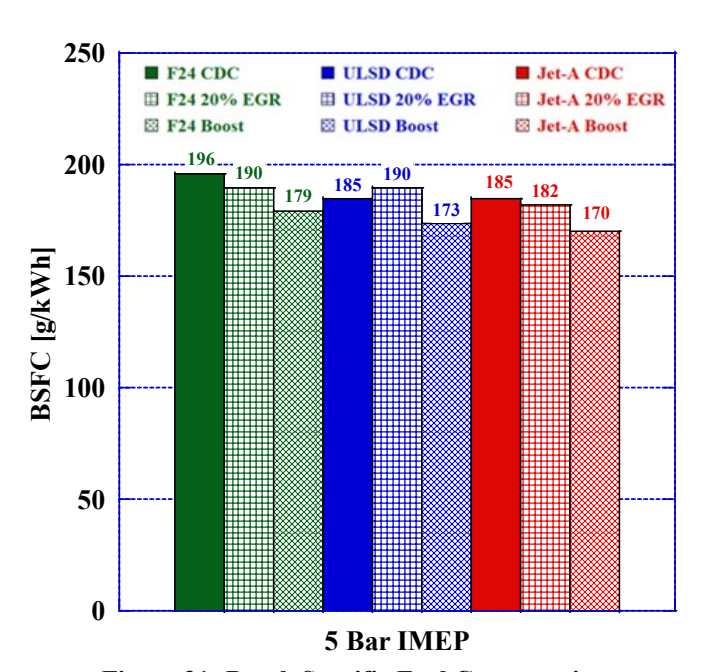


Figure 31: Break Specific Fuel Consumption

Table 14: Direct Injection Fuel Flow Rate

Fuel and Combustion	Fuel Flow [Kg/hr]
Mode	
F24 CDC	1.11
F24 EGR	1.07
F24 Boost	1.01
ULSD CDC	1.04
ULSD EGR	1.07
ULSD Boost	0.98
Jet-A CDC	1.04
Jet-A EGR	1.03
Jet-A Boost	0.96

CONCLUSION

An investigation into the combustion characteristics of F24 and Jet-A was conducted utilizing a common rail direct injection research engine with ULSD as a baseline. Each of the fuels had three combustion experiments, one with no EGR added and no boost added dubbed 'CDC,' one test with 20% EGR added and one with 0.28 bar of boost added. Additionally, the fuels were analyzed for their fundamental combustion characteristics in a PAC CID CVCC. It was discovered that the ID and CD of Jet-A was 12.3% and 6.2% respectively. This was shorter than that of ULSD, resulting in a greater autoignition quality figure (DCN) of 47 (4.3% larger). F24 had a longer period of ID and CD compared to that of ULSD with values 7.4% and 5.7%, respectively, resulting in a lower DCN value of 43.35, or a reduction of 3.7%.

In this study it was discovered that F24 is least effected by the change in EGR or boost added during combustion. F24 has more consistency in its peak pressure rise rate, peak pressures and peak apparent heat release rate than that of ULSD or Jet-A. F24 also had lower values for RI than ULSD or Jet-A for CDC and EGR combustion modes; however, when boost is added F24 resulted in the largest value for RI with increases of 44.4% and 86.4% compared to ULSD and Jet-A respectively.

The emissions output by the aerospace fuels excelled in reductions of Soot. The aviation fuels reduced emissions of NO_X with boost added, with F24 and Jet-A having reductions of 13.8% and 2.1% compared to ULSD.

The break specific fuel consumption (BSFC) for Jet-A was the lowest of all experiments with reductions of 4.3% and 1.75% in EGR and Boost modes, compared to ULSD, and matching the BSFC of ULSD in CDC modes. F24 had increases of 5.8% and 3.5% in CDC and boosted modes for BSFC and had identical amounts for ULSD with EGR added. However, the aerospace fuels produced more emissions across the experiments for CO₂, nearly all experiments for UHC (F24 had a reduction of 3.1% with EGR added compared to ULSD) and nearly all the experiments for CO (F24 had a reduction of 56.7% with the addition of EGR compared to ULSD).

ACKNOWLEDGMENTS

The authors would like to acknowledge David Obando Ortegon and Brianna Leckie of Georgia Southern University for their assistance during the paper writing process. The authors also acknowledge the contribution of the Air Force Laboratory for supplying the experimental fuels, Charles McGuffy from PAC concerning the PAC CID 510, and Joseph Wolfgang from Malvern Lasers. Finally, we would like to acknowledge Richard Smith Jr. P.E. for supporting this endeavor. This paper is based upon work supported by the National Science Foundation Grant No. 1950207.

REFERENCES

- [1] R. G. Papagiannakis, P. N. Kotsiopoulos, D. T. Hountalas, and E. Yfantis, "Single Fuel Research Program comparative results of the use of JP-8 aviation fuel versus diesel fuel on a direct injection and indirect injection diesel engine," SAE Technical Paper Series, 2006.
- [2] D. M. Korres, E. Lois, and D. Karonis, "Use of JP-8 aviation fuel and biodiesel on a diesel engine," SAE Technical Paper Series, 2004. [3] W. Jing, W. L. Roberts, and T. Fang, "Effects of ambient temperature and oxygen concentration on diesel spray combustion using a single-nozzle injector in a constant volume combustion chamber," Combustion Science and Technology, vol. 185, no. 9, pp. 1378–1399, 2013.
- [4] G. Pawlak, T. Skrzek, and P. Płochocki, "The examination of injection strategies of jet propellant-8 for compression ignition engine with a low compression ratio," Fuel Communications, vol. 7, p. 100014, 2021.
- [5] J. Lee, H. Oh, and C. Bae, "Combustion process of JP-8 and fossil diesel fuel in a heavy duty diesel engine using two-color thermometry," Fuel, vol. 102, pp. 264–273, 2012.
- [6] Belvoir, R. D. "E Centre. JP-8 single fuel forward report." US army, 1991
- [7] R. G. Papagiannakis, P. N. Kotsiopoulos, D. T. Hountalas, and E. Yfantis, "Single Fuel Research Program comparative sults of the use of JP-8 aviation fuel versus diesel fuel on a direct injection and indirect injection diesel engine," SAE Technical Paper Series, 2006.
- [8] Church, G. J. (1990). NATO logistics handbook. SNLC Secretariat International Staff, Defence Policy and Planning Division, Logistics NATO HQ, 1110.
- [9] S. J. Lestz and M. E. LePera, "Technology demonstration of U.S. army ground materiel operating on aviation kerosene fuel," SAE Technical Paper Series, 1992.
- [10] G. Labeckas and S. Slavinskas, "Combustion phenomenon, performance and emissions of a diesel engine with aviation turbine JP-8 fuel and rapeseed biodiesel blends," Energy Conversion and Management, vol. 105, pp. 216–229, 2015.

- [11] H. McKee, G. Fernandes, J. Fuschetto, Z. Filipi, and D. Assanis, "Impact of military JP-8 fuel on heavy duty diesel engine performance and emissions," Journal of Automobile Engineering, 2005.
- [12] "USMC policy on converting Conus aviation and ground/tactical equipment from JP-8 to F-24," Home. [Online]. Available: https://www.marines.mil. [Accessed: 09-Jun-2022].
- [13] X. Wang, T. Jia, L. Pan, Q. Liu, Y. Fang, J.-J. Zou, et al. Review on the Relationship Between Liquid Aerospace Fuel Composition and Their Physicochemical Properties Transactions of Tianjin University, 27 (2) (2020), pp. 87-109
- [14] J. Guzman, K. Brezinsky Experimental and modeling study of the oxidation of F-24 jet fuel, and its mixture with an iso-paraffinic synthetic jet fuel, ATJ Combustion and Flame, 224 (2021), pp. 108-125
- [15] T. Damartzis and A. Zabaniotou, "Thermochemical conversion of biomass to second generation biofuels through integrated process design—A review," Renewable and Sust. Energy Reviews, vol. 15, no. 1, pp. 366–378, 2011.
- [16] C. Gutiérrez-Antonio, F. I. Gómez-Castro, J. A. de Lira-Flores, and S. Hernández, "A review on the production processes of renewable jet fuel," Renewable and Sustainable Energy Reviews, vol. 79, pp. 709–729, 2017.
- [17] I. Schifter, C. González-Macías, and I. Mejía-Centeno, "Merit function for simultaneous optimization of fuel properties, naturally aspirated spark-ignition engines equipped with port fuel injection system, and regulated emissions," Fuel, vol. 313, p. 122701, 2022.
- [18] J. Zheng, E. Hu, Z. Huang, D. Ning, and J. Wang, "Combustion and emission characteristics of a spray guided direct-injection sparkignition engine fueled with natural gas-hydrogen blends," International Journal of Hydrogen Energy, vol. 36, no. 17, pp. 11155–11163, 2011.
- [19] Y. Jeihouni, S. Pischinger, L. Ruhkamp, and T. Koerfer, "Relationship between fuel properties and sensitivity analysis of non-aromatic and aromatic fuels used in a single cylinder heavy duty diesel engine," SAE Technical Paper Series, 2011.
- [20] F. K. Tsuji and L. D. Neto, "Influence of Vegetable Oil in the Viscosity of Biodiesel A Review," SAE Technical Paper Series, 2008. doi:10.4271/2008-36-0170.
- [21] ASTM D7668-14a, "Standard Test Method for Determination of Derived Cetane Number (DCN) of Diesel Fuel Oils—Ignition Delay and Combustion Delay Using a Constant Volume Combustion Chamber Method," ASTM International, West Conshohocken, PA, 2014, www.astm.org
- [22] V. Soloiu, J. T. Wiley, R. Gaubert, D. Mothershed, C. Carapia, R. C. Smith, J. Williams, M. Ilie, and M. Rahman, "Fischer-Tropsch coal-to-liquid fuel negative temperature coefficient region (NTC) and low-temperature heat release (LTHR) in a constant volume combustion chamber (CVCC)," Energy, vol. 198, p. 117288, 2020.
- [23] V. Soloiu, R. Smith, A. Weaver, D. Grall, C. Carapia, L. Parker, M. Ilie, M. Rahman, and G. Molina, "Investigations of low-temperature heat release and negative temperature coefficient regions

- of iso-Paraffinic kerosene in a constant volume combustion chamber," ASME 2021 Internal Combustion Engine Division Fall Technical Conference, 2021.
- [24] E. E. Elmalik, B. Raza, S. Warrag, H. Ramadhan, E. Alborzi, and N. O. Elbashir, "Role of hydrocarbon building blocks on gas-to-liquid derived synthetic jet fuel characteristics," Industrial & Engineering Chemistry Research, vol. 53, no. 5, pp. 1856–1865, 2013.
- [25] X. Han, M. Liszka, R. Xu, K. Brezinsky, and H. Wang, "A high pressure shock tube study of pyrolysis of real jet fuel jet a," Proceedings of the Combustion Institute, vol. 37, no. 1, pp. 189–196, 2019.
- [26] J. T. Edwards, "JET FUEL PROPERTIES," https://www.afrl.af.mil/. [Online]. Available: https://apps.dtic.mil/sti/pdfs/AD1093317.pdf. Jan, 2020
- [27] D. Kang, D. Kim, V. Kalaskar, A. Violi, and A. Boehman, "Experimental characterization of jet fuels under engine relevant conditions Part 1: Effect of chemical composition on autoignition of conventional and alternative jet fuels," Fuel, vol. 239, pp. 1388–1404, 2019.
- [28] J. Guzman and K. Brezinsky, "Experimental and modeling study of the oxidation of F-24 jet fuel, and its mixture with an iso-paraffinic synthetic jet fuel, ATJ," Combustion and Flame, vol. 224, pp. 108–125, 2021.
- [29] W. Jing, W. L. Roberts, and T. Fang, "Spray combustion of Jet-A and diesel fuels in a constant volume combustion chamber," Energy Conversion and Management, vol. 89, pp. 525–540, 2015.
- [30] Y. Park, J. Hwang, C. Bae, K. Kim, J. Lee, and S. Pyo, "Effects of diesel fuel temperature on fuel flow and spray characteristics," Fuel, vol. 162, pp. 1–7, 2015.
- [31] V. Soloiu, R. Gaubert, J. Moncada, J. Wiley, J. Williams, S. Harp, M. Ilie, G. Molina, and D. Mothershed, "Reactivity controlled compression ignition and low temperature combustion of Fischer-Tropsch Fuel Blended with n-butanol," Renewable Energy, vol. 134, pp. 1173–1189, 2019.
- [32] Heywood, J. 1988, Internal Combustion Engine Fundamentals, McGraw-Hill, New York.
- [33] B. Rahmanian, M. R. Safaei, S. N. Kazi, G. Ahmadi, H. F. Oztop, and K. Vafai, "Investigation of Pollutant Reduction by simulation of turbulent non-premixed pulverized coal combustion," Applied Thermal Engineering, vol. 73, no. 1, pp. 1222–1235, 2014.
- [34] M. Safaie, B. Rahmanian, and M. Goodarzi, "Investigation of the coal diameter effect on pulverized coal combustion for pollutant reduction," Journal of Mathematics and Computer Science, vol. 12, no. 02, pp. 143–151, 2014.
- [35] V. Rapp, N. Killingsworth, P. Therkelsen, and R. Evans, "Leanburn internal combustion engines," Lean Combustion, pp. 111–146, 2016.

- [36] J. Hwang, Y. Park, C. Bae, J. Lee, and S. Pyo, "Fuel temperature influence on spray and combustion characteristics in a constant volume combustion chamber (CVCC) under simulated engine operating conditions," Fuel, vol. 160, pp. 424–433, 2015.
- [37] D. Kang, D. Kim, V. Kalaskar, A. Violi, and A. Boehman, "Experimental characterization of jet fuels under engine relevant conditions Part 1: Effect of chemical composition on autoignition of conventional and alternative jet fuels," Fuel, vol. 239, pp. 1388–1404, 2019.
- [38] E. Khalife, M. Tabatabaei, A. Demirbas, and M. Aghbashlo, "Impacts of additives on performance and emission characteristics of diesel engines during steady state operation," Progress in Energy and Combustion Science, vol. 59, pp. 32–78, 2017.
- [39] Q. Fang, J. Fang, J. Zhuang, and Z. Huang, "Effects of ethanol-diesel-biodiesel blends on combustion and emissions in premixed low temperature combustion," Applied Thermal Engineering, vol. 54, no. 2, pp. 541–548, 2013.
- [40] D. B. Hulwan and S. V. Joshi, "Performance, emission and combustion characteristic of a multicylinder di diesel engine running on diesel–ethanol–biodiesel blends of high ethanol content," Applied Energy, vol. 88, no. 12, pp. 5042–5055, 2011.
- [41] R. Vallinayagam, S. Vedharaj, W. M. Yang, C. G. Saravanan, P. S. Lee, K. J. E. Chua, and S. K. Chou, "Impact of ignition promoting additives on the characteristics of a diesel engine powered by Pine Oil–Diesel blend," Fuel, vol. 117, pp. 278–285, 2014.
- [42] Valentin Soloiu, Amanda Weaver, Lily Parker, Austin Brant, Richard Smith, Marcel Ilie, Gustavo Molina, Cesar Carapia, "Constant volume combustion chamber (CVCC) investigations of aerospace F-24 and Jet-A in low-temperature heat release and negative temperature coefficient regions," *Energy Conversion and Management*, Volume 263, 2022, 115687, ISSN 0196-8904, https://doi.org/10.1016/j.enconman.2022.115687.